PAPER • OPEN ACCESS

Comparison between the NMPC and EOR control of wind turbines using LIDAR wind measurements

To cite this article: Amin Mahdizadeh *et al* 2018 *J. Phys.: Conf. Ser.* **1037** 032046

View the article online for updates and enhancements.

IOP ebooks™

Bringing you innovative digital publishing with leading voices to create your essential collection of books in STEM research.

Start exploring the collection - download the first chapter of every title for free.

Comparison between the NMPC and EOR control of wind turbines using LIDAR wind measurements

Amin Mahdizadeh[1]**, Elham Tofighi**[2]**, Robert Schmid**[1]

[1]Department of Electrical and Electronic Engineering, University of Melbourne, Victoria 3010, Australia
[2]School of Electrical Engineering and Computer Science, University of Newcastle, Callaghan NSW 2308, Australia

E-mail: `amahdizadeh@student.unimelb.edu.au`

Abstract.
    The upstream wind is known as the main source of disturbance to the wind turbine. Therefore, having the wind information before it hits the turbine, allows the wind turbine controller to take necessary actions to proper rejection of the disturbances. Several advanced control methods have been proposed to exploit the LIDAR wind measurements to enhance the wind turbine control. To date, the Nonlinear Model Predictive Control (NMPC), has been one of the most successful methods in using wind data to improve the control performance. However, due to the immense computational burden, its real-time application is still challenging. Very recently, an implementation of the Exact Output Regulation (EOR) scheme for wind turbines control has been proposed. In this paper, the performances of the two model-based controllers, namely the NMPC controller and the EOR controller, in mitigating mechanical loads on the DTU10MW wind turbine are compared against each other. The results are also compared against the classic baseline feedback controller. Simulation results indicate that both controllers show significant improvement in reducing fatigue loads on the wind turbine structure, whilst maintaining the power production at the desired rated level in comparison to the baseline controller. It is also shown that the EOR controller can closely compete with the disturbance rejection performance of the NMPC controller. The simulation running times are considerably lower for the EOR scheme, potentially making EOR more suitable for real-time applications.

1. Introduction

The classic baseline controller consists of a torque controller and a proportional integral (PI) controller that regulate the wind turbine rotor/generator speed against varying wind conditions. The baseline controller uses a measurement of the rotor/generator speed as the feedback signal and the closed-loop characteristics are achieved by selecting proper PI gains [8, 10, 14]. Although the feedback control has its advantages, e.g., simple design, tuning, and implementation, it is not an optimal approach to wind turbine control since it can only generate delayed control signals that might cause additional loads on the turbine [11]. Over the past few years, several modern control techniques that utilize the LIDAR wind measurements have evolved addressing the problem of disturbance rejection and load reduction [7, 17, 21, 25].

    Wind turbines are generally designed to operate with wind speeds above rated in full-load operation mode [5]. In full-load operation region, the wind turbine operates at its nominal power production capacity while being exposed to high wind speeds that cause large aerodynamic forces on the turbine structure. Varying aerodynamic forces induce fatigue loads on the flexible components of the wind

1

turbine. Hence, it is critical to ensure that the wind turbine control system is capable of steering the wind turbine and alleviating the loads [10].

Present work provides a detailed performance comparison between two advanced wind turbine control schemes; Nonlinear Model Predictive Control (NMPC), and Exact Output Regulation (EOR). These controllers are designed to utilize the LIDAR wind measurements and control the full aero-elastic model of the DTU10MW wind turbine model in FAST. NMPC is capable of utilizing the LIDAR wind measurements to predict the future behavior of the system and compute optimal solutions [18, 21, 24]. On the other hand, EOR [16] is a more analytic feed-forward control approach which calculates the control input by approximating the LIDAR measurements into low-order exo-systems. The performance of both methods will be compared against that obtained from the classic baseline linear feedback controller [15] to assess the advantages of utilizing wind preview information in improving the performance of the wind turbine control.

The remainder of the paper is organized as follows: In Section 2 a brief introduction to wind turbine and wind field modeling are provided. The wind turbine control principles are explained in Section 3 and the NMPC and EOR controllers introduced. The simulation results, comparisons and analysis are provided in Section 4, and finally the conclusion and outlook are summarized in Section 5.

2. Mathematical modeling & configuration

Specialized aero-elastic models (e.g., FAST [13]) have been developed to model the wind turbines such that their intricate characteristics are replicated. These models enable the analysis of different aspects of wind turbine behavior over wide ranges of wind speeds and operating modes. However, they are too complicated to be utilized in model-based control design applications. Hence, simplified mathematical models that exhibit dominant characteristics and behavior of wind turbines are developed and implemented in modern model-based controller design [4]. In this paper, the DTU10MW Reference Wind Turbine is considered. This wind turbine is developed as part of the Light Rotor project through cooperation between the DTU Wind Energy and Vestas [3] and is based on the IEC Class I-A wind climate [1]. Full description of the DTU10MW RWT parameters and specifications can be found in [6].

2.1. Simplified low-order model of the DTU10MW wind turbine

The simplified LOW-Order Wind Turbine Model (SLOW) for the DTU10MW is developed using the finite-element-based multi-body dynamic analysis for modeling of the aero-elastic systems [4, 20]. The SLOW model provides a low-order closed-form mathematical description of the horizontal axis wind turbines and can be employed in wind turbine system-level modeling and analysis. The proposed SLOW model consists of the aerodynamic sub-system, the structural sub-system, and the actuator sub-system.

The wind turbine rotor captures the kinetic energy in the moving air and converts it into mechanical work, i.e., aerodynamic torque, M_a, on the rotor shaft and the thrust force, F_a, on the tower. The aerodynamic sub-system is given as:

$$M_a(\Omega, \dot{x}_T, \theta, \upsilon_0) := \frac{1}{2}\rho\pi R^3 \frac{c_P(\lambda, \theta)}{\lambda} \upsilon_{\text{rel}}^2, \tag{1a}$$

$$F_a(\Omega, \dot{x}_T, \theta, \upsilon_0) := \frac{1}{2}\rho\pi R^2 c_T(\lambda, \theta) \upsilon_{\text{rel}}^2, \tag{1b}$$

where R and ρ denote the wind turbine rotor radius and the air density at the hub height. The tip speed ratio, $\lambda = \frac{\Omega R}{\upsilon_{rel}}$ defines the ratio between the tangential speed of each blade tip to the mean wind speed at the rotor cross-section and the relative wind speed, is calculated as $\upsilon_{\text{rel}} := \upsilon_0 - \dot{x}_T$.

The aerodynamic torque, M_a, and the aerodynamic thrust, F_a, are nonlinear functions of the effective power coefficient $c_P(\lambda, \theta)$ and thrust force coefficient, $c_T(\lambda, \theta)$. In this paper, these parameters are generated for the DTU10MW reference wind turbine using the steady-state simulations on the full nonlinear model of the turbine in FAST and are stored in look-up tables.

The structural sub-system consists of the drive-train and tower dynamics:

$$J\dot{\Omega} + \frac{M_g}{i_{gb}} = M_a(\dot{x}_T, \Omega, \theta, \upsilon_0), \tag{2a}$$

$$m_{Te}\ddot{x}_T + c_{Te}\dot{x}_T + k_{Te}(x_T - x_{T0}) = F_a(\dot{x}_T, \Omega, \theta, \upsilon_0), \tag{2b}$$

where J is the sum of the total moment of inertia of the drive-train about the rotor shaft, $\dot{\Omega}$ is the rotor angular acceleration, and M_g is the generator torque. The coefficients, m_{Te}, c_{Te}, and k_{Te} denote the sum of the mass of the tower components, the tower damping, and the tower stiffness respectively.

The actuator sub-system consists of the blade pitch actuator and the generator torque actuator. The blade servo system dynamics are modeled as a linear second-order system that connects the pitch command signal, θ_c, to the actual blade pitch angle, θ:

$$\ddot{\theta} + 2\zeta\omega_{PA}\dot{\theta} = \omega_{PA}^2(\theta_c - \theta), \tag{3}$$

where ζ denotes the damping factor, ω_{PA} is the undamped natural frequency of the blade pitch actuator and θ_c is the collective blade pitch reference signal.

In electro-mechanical systems, the dynamics of electrical components are significantly faster than the dynamics of mechanical/structural parts. Hence, it is safe to assume that the actual generator torque, M_g, directly tracks the reference electromagnetic torque.

2.2. Wind measurement model

Over the past few years, LIDAR (light detection and ranging) technology has emerged to play an effective role in improving the performance of wind turbine controllers in increasing the wind energy harvest whilst reducing the mechanical loads on the turbine components [23]. Nacelle-mounted LIDAR systems use laser beams to scan the space in front of the turbine, collect the information on the moving air, analyze it, and construct relatively accurate hub-height rotor effective wind speed trajectories for the wind turbine control system. The wind turbine control utilizes this information to take pre-emptive actions to reject the effects of disturbances on the wind turbine [22]. In this paper, the wind preview measurements, to be used by the controller, are generated using the LIDAR Simulator described in [20].

3. Variable speed control of wind turbines
3.1. Wind turbine control principles
The main objective in control of wind turbines is to ensure that the maximum wind energy is extracted whilst the structural loads are contained [5]. Most of modern utility-scale wind turbines are designed to operate in full-load operation region. As the name suggests, wind turbines are exposed to high levels of loading in this operation mode. Hence, it is critical for the wind turbine controller to actively alleviate the loads on the turbine structure [11].

3.2. Sampled-data Nonlinear Model Predictive Control (NMPC) for wind turbines
Sampled-data NMPC [2] is based on the solution of a finite horizon open-loop Optimal Control Problem (OCP). At every sampling instant, ($t_k = k\delta$, $k \in \mathbb{N}$ and $\delta > 0$), the controller computes a sequence of control signals, $u(\cdot)$, such that the cost function, J_{OCP}, is minimized over the prediction horizon, $T_p \in \mathbb{R}^+$.

With the wind measurements available via LIDAR over the prediction horizon, T_p, the mathematical formulation of the OCP may be written as:

$$\underset{\hat{u}(\cdot)}{\text{minimize}}\, J_{\text{OCP}}(x(t_k), \hat{u}(\cdot), \hat{d}(\tau); T_p) = \frac{1}{T_p}\int_{t_k}^{t_k+T_p} \ell(\hat{x}(\tau), \hat{u}(\tau), \hat{d}(\tau))d\tau, \tag{4a}$$

subject to $\forall \tau \in [t_k, t_k + T_p]$:

$$\dot{\hat{x}}(\tau) = f(\hat{x}(\tau), \hat{u}(\tau), \hat{d}(\tau)), \quad \hat{x}(t_k) = x(t_k), \tag{4b}$$

$$0 \geq g_i(\hat{x}(\tau), u(\tau), \hat{d}(\tau)), \quad i = 1 \ldots, n_g \tag{4c}$$

$$u(\tau) \in \mathscr{U}, \tag{4d}$$

where $\ell(\hat{x}(\tau), \hat{u}(\tau), \hat{d}(\tau)) : \mathbb{R}^{m_u} \times \mathbb{R}^{n_x} \times \mathbb{R}^{n_d} \longrightarrow \mathbb{R}_0^+$ is the objective function and specifies the system performance criteria with respect to the operational, economical and ecological considerations.

The function $f(\hat{x}(\tau), \hat{u}(\tau), \hat{d}(\tau))$ in (4b) defines the equality constraints while $g_i(\hat{x}(\tau), u(\tau), \hat{d}(\tau))$ in (4c) represents the nonlinear inequality constraints on states and inputs. In (4d), $\mathscr{U} := \{u \in \mathbb{R}^m | u_{min} \leq u \leq u_{max}\}$ is included to ensure that the control commands are bounded within a given set of limits that are generally defined by physical properties and characteristics of the wind turbine actuators.

The optimal solution to the OCP in (4) is computed repeatedly at the sampling instances $t_k = k\delta$, $k = 0, 1, ..., N_p$ yielding sequences of control trajectories $u^\star(\cdot; x(t_k)) : [t_k, t_k + T_p] \longrightarrow \mathscr{U}$. The closed-loop control input is then selected as the first segment of each control sequence and is applied to the system at current sampling interval as

$$u(\tau) := u^\star(\tau; x(t_k)), \quad \forall \tau \in [t_k, t_{k+1}). \tag{5}$$

The NMPC cost function, ℓ, is designed to reflect the classic wind turbine control goals to mitigate extreme and fatigue loads while the generated power is maximized:

$$
\begin{aligned}
\ell(\hat{x}(\tau), u(\tau), \hat{d}(\tau), \tau) = {} & q_1(v_0(\tau)) \left(\Omega(\tau) - \Omega_{\mathrm{ref}}(\tau)\right)^2 \\
& + q_2 \left(\dot{x}(\tau)\right)^2 \\
& + q_3(v_0(\tau)) \left(M_g(\tau) - M_{g,\mathrm{ref}}(\tau)\right)^2 \\
& + q_4(v_0(\tau)) \left(\dot{\theta}(\tau)\right)^2 \\
& + q_5 \left(\dot{M}_g(\tau)\right)^2 \\
& + q_6(v_0(\tau)) \left(\theta_c(\tau)\right)^2,
\end{aligned}
\tag{6}
$$

where $q_k > 0$ with $k \in \{1, 2, ..., 6\}$ denotes the set of weights that are selected to penalize and/or regulate the wind turbine behavior against the variable wind speed.

It can be realized that except for the rotor speed, Ω, and the electromagnetic torque, M_g, the cost function terms are regulated to the equilibrium point in the origin. The choice of the reference rotor speed trajectory, Ω_{ref}, depends on the wind speed, v_0. For above rated wind speeds, the controller attempts to maintain the rated rotor speed and therefore, $\Omega_{\mathrm{ref}}(\tau) = \Omega_{\mathrm{rated}}$.

Furthermore, the generated torque, M_g, is penalized against the reference generator torque, $M_{g,\mathrm{ref}}$, which aims to limit the electrical power to the nominal value, $P_{el,\mathrm{rated}}$, in full-load operation region:

$$M_{g,\mathrm{ref}}(\tau) = \frac{P_{el,\mathrm{rated}}}{\eta_{el}\Omega_g}. \tag{7}$$

To prevent saturation of the system actuators, hardware constraints are applied on input signals. Hence, the generator torque actuation rate, $\dot{M}_g$, is limited by

$$\dot{M}_g \in [-\dot{M}_{g,\mathrm{max}}, +\dot{M}_{g,\mathrm{max}}]. \tag{8}$$

The nonlinear inequality state constraints are also considered on the rotor speed, Ω, the blade pitch angle, θ, and the blade pitch rate, $\dot{\theta}$:

$$
\begin{aligned}
& \Omega \leq 1.2\Omega_{\mathrm{rated}} \\
& \theta_{\mathrm{min}} \leq \theta \leq \theta_{\mathrm{max}} \\
& \dot{\theta} \in [-\dot{\theta}_{\mathrm{max}}, +\dot{\theta}_{\mathrm{max}}].
\end{aligned}
\tag{9}
$$

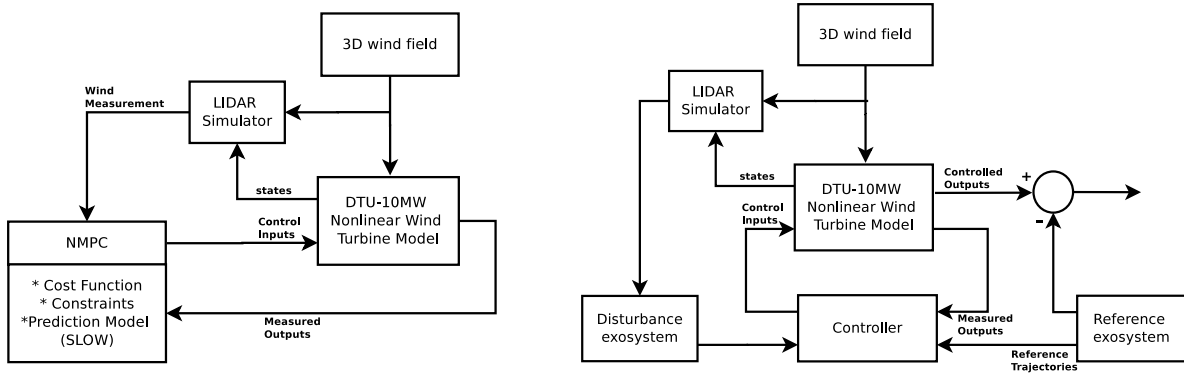The proposed sampled-data NMPC control is depicted in Figure 1(left).

Figure 1. Schematic block-diagram of the NMPC controller (Left) and the EOR controller (Right)

3.3. Exact Output Regulation (EOR) for wind turbines

The EOR controller is constructed based on the assumption that both the disturbance and the reference signals are known in advance and can be generated by autonomous exo-systems. Although this is an strong assumption for practical applications, it is valid since the LIDAR is used to measure the future disturbance signals. The fundamentals of the EOR method used in this paper are discussed in [19] and the adaptation of the EOR to the LIDAR-assisted wind turbine control is presented in [16] where the plant and control are described by the multi-variable linear system with the following state equations:

$$\Sigma : \begin{cases} \dot{x}(t) &= Ax(t) + Bu(t) + Hd(t) \\ z(t) &= C_z x(t) \\ y(t) &= Cx(t), \end{cases}$$

where $u(t)$, $z(t)$, and $y(t)$ are the control input, measured, and controlled output vectors respectively. As mentioned earlier, the reference and disturbance signals can be shown by the output of two autonomous exo-systems as:

$$\Sigma_{exo,1} : \begin{cases} \dot{\eta}(t) = S_1 \eta(t) & \eta(0) = \eta_0 \\ d(t) = L_1 \eta(t), \end{cases} \tag{10}$$

and

$$\Sigma_{exo,2} : \begin{cases} \dot{\zeta}(t) = S_2 \zeta(t) & \zeta(0) = \zeta_0 \\ r(t) = L_2 \zeta(t), \end{cases} \tag{11}$$

where for all $t \leq 0$, $\eta(t) \in R^{n_1}$ and $\zeta(t) \in R^{n_2}$ are the internal states of the harmonic generators that act as the exo-systems. The dimensions n_1 and n_2 are the orders of exo-systems which are determined with respect to the number of harmonics that are required for a suitable approximation of LIDAR measurements. Estimation of the matrices S and L is explained in [16]. Here, the control objective is to ensure that the controlled output, $y(t)$, asymptotically tracks the reference signal, $r(t)$, while the effect of the disturbance, $d(t)$, is rejected. The error between the controlled output and the reference is defined as $e(t) := y(t) - r(t)$.

The error system, Σ_e, is obtained from Σ, where the output $y(t)$ is replaced by $e(t)$:

$$\Sigma_e : \begin{cases} \dot{x}(t) &= Ax(t) + Bu(t) + Hd(t) \\ z(t) &= C_z x(t) + D_z u(t) \\ e(t) &= Cx(t) + Du(t) - r(t). \end{cases} \tag{12}$$

The exact output regulation problem is then translated as finding a control law, u, for Σ_e to ensure that (i) the closed-loop system is stable when $d = 0$, and (ii) $\lim_{t \to \infty} e(t) = 0$.

The exo-systems may be re-written in the compact form:

$$\Sigma_{exo} : \begin{cases} \dot{w} = Sw(t), \quad w(0) = w_0 \\ \begin{bmatrix} d(t) \\ r(t) \end{bmatrix} = \begin{bmatrix} L_1 & 0 \\ 0 & L_2 \end{bmatrix} w(t), \end{cases} \tag{13}$$

where $S := \begin{bmatrix} S_1 & 0 \\ 0 & S_2 \end{bmatrix}$ and $w(t) := \begin{bmatrix} \eta(t) \\ \zeta(t) \end{bmatrix}$.

Assuming full-state feedback, it can be said that $z = x$. The error system Σ_e is then be re-written as

$$\Sigma_e : \begin{cases} \dot{x}(t) &= A x(t) + B u(t) + E_w w(t), \quad x(0) = x_0 \\ \dot{w}(t) &= S w(t), \quad w(0) = w_0 \\ e(t) &= C x(t) + D u(t) + D_{ew} w(t), \end{cases} \tag{14}$$

where

$$E_w \overset{\text{def}}{=} \begin{bmatrix} H L_1 & 0 \end{bmatrix}$$
$$D_{ew} \overset{\text{def}}{=} \begin{bmatrix} 0 & -L_2 \end{bmatrix}.$$

Finally, the control input signal for Σ_e is be calculated from

$$u(t) = Fx(t) + Gw(t), \tag{15}$$

where F is the state feedback matrix and is determined with respect to the desired pole locations by means of any pole placement method. Once F has been selected, the feed-forward gain matrix, G, can be calculated by solving the regulator equations as given in the following theorem:

Theorem 3.1 *([19], Theorem 2.3.1) Assume system Σ_e in (14) satisfies the following assumptions*

(A.1) The pair (A,B) is stabilizable.

(A.2) The matrix S is anti-Hurwitz-stable.

(A.3) There exists matrices Γ and Π satisfying

$$\Pi S = A\Pi + B\Gamma + E_w \tag{16}$$
$$0 = C\Pi + D\Gamma + D_{ew}. \tag{17}$$

Let F be any matrix such that $A + BF$ is Hurwitz-stable, and let $G = \Gamma - F\Pi$. Then u as in (15) achieves exact output feedback regulation for Σ_e.

4. Simulation results and Analysis

In this section, the performance of the proposed NMPC and EOR controllers in achieving the wind turbine control objectives for all wind speed above rated (in full-load operation region) are compared against each other. For a more comprehensive study, the results are also compared to a baseline controller. The baseline controller is an adaptation of the feedback PI controller introduced in [15]. In this controller, the generator speed, Ω_g, is measured as the feedback signal for the blade-pitch PI controller and the generator torque attempts to keep the generated power as rated and therefore, $M_g = \frac{P_{el,\text{rated}}}{\Omega_g}$.

For realistic aero-elastic simulations, the full nonlinear model of a single on-shore DTU10MW wind turbine in FAST [3] is considered. The simplified model, for controller design, is based on SLOW model introduced in Section 2.1. A full state feedback is assumed and consequently no state estimators are required.

The NMPC controller is set-up based on the configurations in [24]. The prediction horizon, T_p, is set to 5.6 seconds and the inputs are parameterized piecewise constant with 28 equally-spaced time
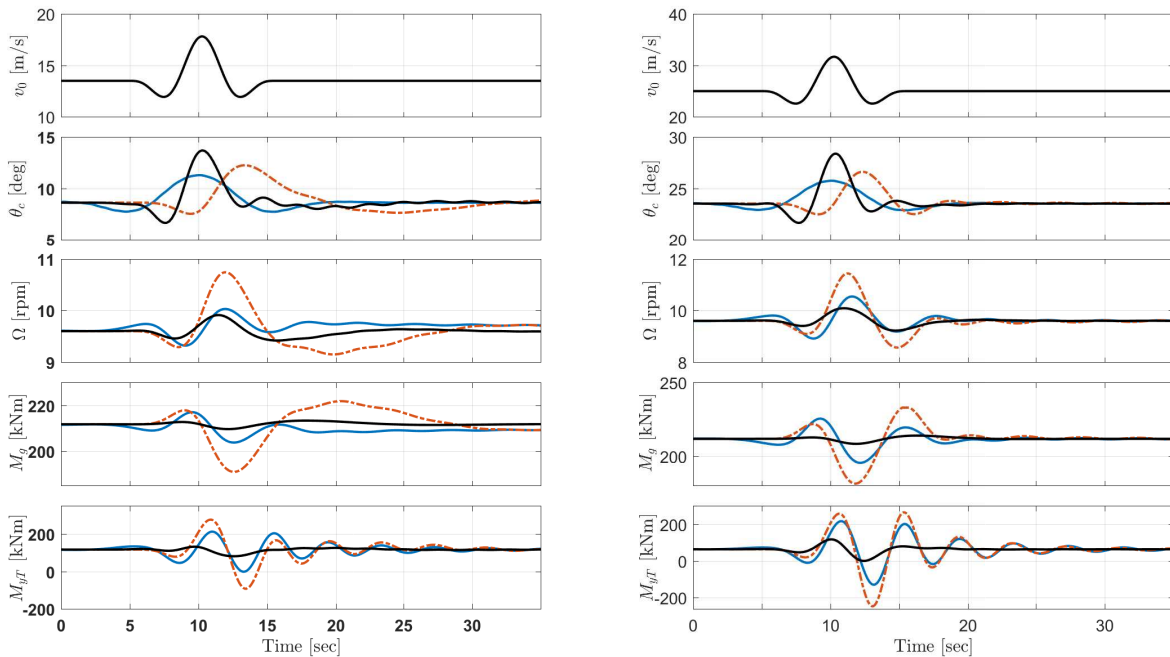
Figure 2. Simulation results for the extreme operation conditions with the full aero-elastic model in FAST. Left: EOG13.5m/s, Right: EOG25m/s. Baseline controller (Red), NMPC controller (Black), EOR controller (Blue).

intervals over the prediction horizon ($\delta = 0.2$ seconds). At the simulation start point, it is assumed that the wind turbine operates in steady-state mode and therefore the initial state variables for the NMPC are accordingly. The OCP in (4) is solved using the nonlinear programming, the single direct shooting with the sequential quadratic programming (SQP)/trust-region method implemented in MATLAB®. The integrations to solve the nonlinear model of the wind turbine is performed using the fourth-order Runge-Kutta method.

The EOR controller is based on the design method and configurations described in [16]. Here, the same wind preview information of 5.6 seconds is fed to the controller. The feed-forward matrix G is calculated by the EOR algorithm and the feedback matrix F is chosen to place the closed-loop poles at: $P_{cl} = [-0.0535 \pm 2.0572i, 0.1415, -3.0699 \pm 3.0265i$.

It should also be mentioned that due to space limitations, the performance of the proposed NMPC and EOR-based controllers are only studied in the full-load operation.

4.1. Extreme load analysis

In the time-domain it is essential to assess the performance of the proposed controllers against the gust events. Assuming perfect wind measurements, the hub-height time-series are created with extreme operation gusts according to the IEC standard [1] at $v_{rated} + 2$ m/s $= 13.2$ m/s and $v_{out} = 25$ m/s. The wind speeds EOG13.5 m/s and EOG25 m/s are fed to the FAST model of the DTU10MW as well as the NMPC- and EOR-based controllers. Figure 2 summarizes the simulation results and compares the pitch angle, θ_c, rotor speed, Ω, generator torque, M_g, and the tower base foreaft bending moment, $M_{y,T}$ for the baseline, NMPC and the EOR-based controllers.

For both extreme wind speeds at EOG13.5m/s and EOG25m/s, the NMPC and EOR controllers are able to reduce the rotor speed deviation from the rated value compared to the baseline controller which does not have access to the preview wind measurements. Moreover, the NMPC controller utilizes the generator torque, M_g, to reduce the tower fore-aft oscillations due to its competence to incorporate

Table 1. Performance comparison: Peak values derived from the simulations for extreme operation conditions shown in Figure 2

	EOG 13.5 m/sec		EOG 25 m/sec	
	$M_{yT,\max}$[M Nm]	$\Delta\Omega_{\max}$ [rpm]	$M_{yT,\max}$[M Nm]	$\Delta\Omega_{\max}$[rpm]
NMPC-based control	132	0.55	181	0.86
EOR-based control	150	0.71	210	1.63
Baseline PI controller	276	1.59	265	2.869

multi-variable control. The performance of the proposed controllers in mitigating the extreme loads on the wind turbine tower are summarized in Table 1. It can be see that the performance of the NMPC controller in rejecting the effects of the extreme gust events is higher. This can be explained as it is capable of employing more blade pitch actuation during the gust events.

4.2. Fatigue load analysis
To evaluate the performance of these controllers in reducing the fatigue loads on the wind turbine structure, a set of A-type turbulent wind fields in full-load operation region (generated by TurbSim [12]) is used each with the length of 600 seconds. As the analysis are limited to the control performance for above-rated wind speeds, the wind fields are generated for the mean wind speed of 14, 16, 18, 20, 22, 24 m/s. The wind Fields are also scanned by the LIDAR simulator to generate line-of-sight rotor effective wind profiles for the controllers. Several simulations were run and the life-time damage equivalent loads (DEL) for the tower fore-aft bending moment, M_{yT}, and the low speed shaft torsion, M_{LSS}, were computed. The simulation results, as time-series of the blade pitch angle, θ_c, the out-of-plane blade bending moment, M_{Oop}, rotor speed, Ω, generator torque, M_g, the low speed shaft torsion, , M_{LSS}, the tower fore-aft bending moment, M_{yT}, are shown in Figure 3 for the turbulent winds with the mean wind speed of 16 and 24 m/s. It can be realized that under normal operation conditions, the performance of the EOR and NMPC controllers yield close behavior in the wind turbine.

Furthermore, the fatigue load analysis and calculated DELs (based on the IEC DLC1.2, [9]) are summarized in Figure 4. As it can be seen, both the NMPC and EOR controllers outperform the feedback-only baseline controller with regards to mitigating the fatigue loads on the tower base and the drive-train. However, the EOR controller performs better in reducing the drive-train torsion compared to the NMPC.

Additionally, the recorded simulation run-times show that computational resources for the NMPC controller are considerably higher than EOR and it was not possible to execute NMPC in real-time with the hardware which was used for the simulations. However, the EOR was executed approximately twice as fast as a real-time application using the same hardware.

5. Discussion & Conclusion
The performance of the sampled-data NMPC and EOR controllers are compared against the conventional feedback PI controller in full-load operation region. The NMPC and EOR techniques utilize the future wind information (provided by LIDAR) to reduce the impact of wind disturbances on the turbine operation and alleviate the fatigue loads on the turbine structure. It is shown that both controllers outperform the feedback PI controller in reducing the structural fatigue and extreme loads on the tower and the drive-train.

Furthermore, due to considerably lower computation loads, the EOR controller may be implemented in real-time applications using conventional industrial hardware while implementation of the NMPC controller is not feasible and requires much powerful hardware. Additionally, the NMPC controller is more successful in damping the effects of the extreme operation conditions where it reduces the maximum extreme loads by 52% for the EOG13.3 m/s and 32% for the EOG25 m/s while the EOR
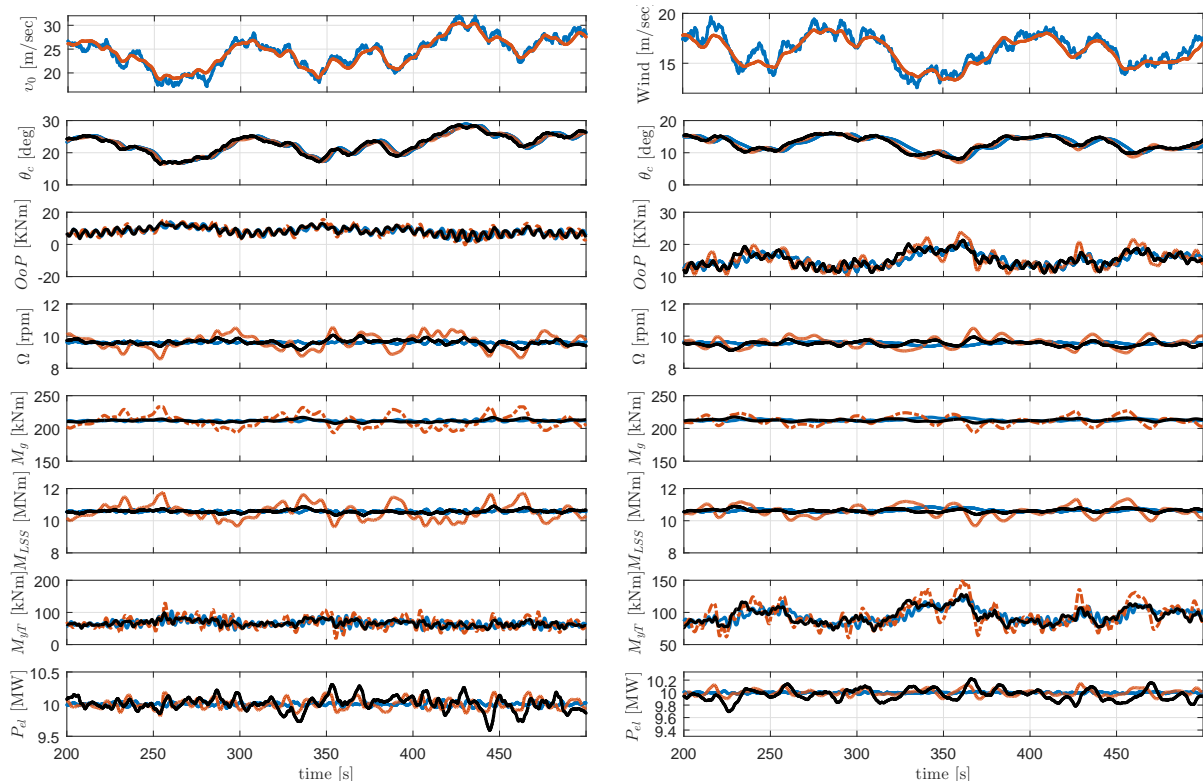
Figure 3. Selected window of simulation results for the normal operation conditions with the full aero-elastic model in FAST. Left: turbulent wind (mean wind speed 24 m/s), Right: turbulent wind (mean wind speed 16 m/s). Baseline controller (Red), NMPC controller (Black), EOR controller (Blue).

controller demonstrates a performance improvement of 45% for the EOG13.3 m/s and 20% for the EOG25 m/s in comparison to the feedback PI controller.

Under normal operation conditions, the EOR controller results in slightly better performance in reducing the fatigue loads compared with the PI controller. The EOR reduces the average fatigue loads on the tower fore-aft bending moment, DEL-M_{yT}, by 47% and the average fatigue loads on the drvietrain, DEL-M_{LSS}, by 81%. The NMPC on the other hand, reduces the average fatigue loads on the tower fore-aft bending moment, DEL-M_{yT}, by 42% and the average fatigue loads on the drvietrain, DEL-M_{LSS}, by 75%.

Future works will focus on examining the performance of the proposed controllers in handling the wind turbine in partial and transition operation regions.

References

[1] IEC 61400-1. Third editions. 2005–2008 Wind Turbines – Part 1: Design Requirements, 2005.

[2] Frank Allgower, Rolf Findeisen, Zoltan K Nagy, et al. Nonlinear model predictive control: from theory to application. *Journal-Chinese Institute Of Chemical Engineers*, 35(3):299–316, 2004.

[3] C Bak, F Zahle, R Bitsche, T Kim, A Yde, LC Henriksen, PB Andersen, A Natarajan, and MH Hansen. Description of the dtu 10 mw reference wind turbine. dtu wind energy report-i-0092. *Technical University of Denmark, Fredericia (Denmark)*, 2013.

[4] Carlo L Bottasso, Alessandro Croce, Barbara Savini, Walter Sirchi, and Lorenzo Trainelli. Aero-servo-elastic modeling and control of wind turbines using finite-element multibody procedures. *Multibody System Dynamics*, 16(3):291–308, 2006.

[5] Tony Burton, David Sharpe, Nick Jenkins, and Ervin Bossanyi. *Wind energy handbook*. John Wiley & Sons, 2011.

[6] Lead Beneficiary DNV GL and Status Final. Qualification of innovative floating substructures for 10mw wind turbines and water depths greater than 50m. 2015.
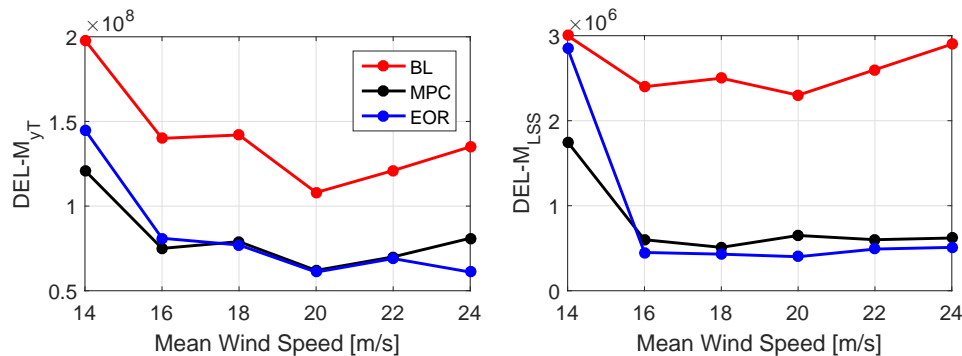
Figure 4. Left: DELs for the tower-bottom fore-aft bending moment, M_{yT}, Right: DELs for the drive-train torsion, M_{LSS}. Baseline controller (Red), NMPC controller (Black), EOR controller (Blue)

[7]   Michael Harris, Maureen Hand, and A Wright. Lidar for turbine control. *National Renewable Energy Laboratory, Golden, CO, Report No. NREL/TP-500-39154*, 2006.
[8]   E N Hinrichsen. Controls for variable pitch wind turbine generators. *IEEE Transactions on Power Apparatus and Systems*, PAS-103(4):886–892, 1984.
[9]   IEC Std., Rev. *IEC 61400-1 third edition 2005-08 Wind turbines - Part 1: Design requirements*. IEC Std., Rev., 2005.
[10] Craig C Johnson and RT Smithior. Dynamics of wind generators on electric utility networks. *IEEE Transaction on Aerospace and Electronic Systems*, AES-12(4):483–493, 1976.
[11] Kathryn E Johnson, Lucy Y Pao, Mark J Balas, and Lee J Fingersh. Control of variable-speed wind turbines: standard and adaptive techniques for maximizing energy capture. *IEEE control systems*, 26(3):70–81, 2006.
[12] Bonnie J Jonkman. Turbsim user's guide: Version 1.50. Technical report, National Renewable Energy Laboratory Colorado, 2009.
[13] Jason M Jonkman, Marshall L Buhl Jr, et al. Fast users guide. *National Renewable Energy Laboratory, Golden, CO, Technical Report No. NREL/EL-500-38230*, 2005.
[14] J M Kos. On-line control of a large horizontal axis wind energy conversion system and its performance in a turbulent wind environment. In *13th Intersociety Energy Conversion Engineering Conference*, volume 1, pages 2064–2073, 1978.
[15] Frank Lemmer, Florian Amann, Steffen Raach, and David Schlipf. Definition of the swe-triplespar floating platform for the dtu 10mw reference wind turbine. *University of Stuttgart*, 2016.
[16] Amin Mahdizadeh, Robert Schmid, and Denny Oetomo. Fatigue load mitigation in multi-megawatt wind turbines using output regulation control. In *System Theory, Control and Computing (ICSTCC), 2017 21st International Conference on*, pages 163–168. IEEE, 2017.
[17] Torben Mikkelsen, Kasper Hjorth Hansen, Nikolas Angelou, Mikael Sjöholm, Michael Harris, Paul Hadley, Richard Scullion, Gary Ellis, and G Vives. Lidar wind speed measurements from a rotating spinner. In *2010 European Wind Energy Conference and Exhibition*, 2010.
[18] Mohammad Mirzaei, Lars Christian Henriksen, Niels Kjolstad Poulsen, Hans Henrik Niemann, and Morten H Hansen. Individual pitch control using lidar measurements. In *Control Applications (CCA), 2012 IEEE International Conference on*, pages 1646–1651. IEEE, 2012.
[19] Ali Saberi, Anton A Stoorvogel, and Peddapullaiah Sannuti. *Control of linear systems with regulation and input constraints*. Springer Science & Business Media, 2012.
[20] David Schlipf. Lidar-assisted control concepts for wind turbines. 2016.
[21] David Schlipf, Dominik Johannes Schlipf, and Martin Kühn. Nonlinear model predictive control of wind turbines using lidar. *Wind Energy*, 16(7):1107–1129, 2013.
[22] David Schlipf, Juan José Trujillo, Valeria Basterra, and Martin Kühn. Development of a wind turbine lidar simulator. In *In Proc. EWEC*, 2009.
[23] Eric Simley, Lucy Y Pao, Neil Kelley, Bonnie Jonkman, and Rod Frehlich. Lidar wind speed measurements of evolving wind fields. In *Proc. AIAA Aerospace Sciences Meeting*, 2012.
[24] Elham Tofighi, Timm Faulwasser, and Christopher M Kellett. Nonlinear model predictive control approach for structural load mitigation of wind turbines in presence of wind measurement uncertainties. In *Control Conference (AUCC), 2015 5th Australian*, pages 210–214. IEEE, 2015.
[25] Elham Tofighi, David Schlipf, and Christopher M Kellett. Nonlinear model predictive controller design for extreme load mitigation in transition operation region in wind turbines. In *Control Applications (CCA), 2015 IEEE Conference on*, pages 1167–1172. IEEE, 2015.

Author/s:
Mahdizadeh, A; Tofighi, E; Schmid, R

Title:
Comparison between the NMPC and EOR control of wind turbines using LIDAR wind measurements

Date:
2018-01-01

Citation:
Mahdizadeh, A., Tofighi, E. & Schmid, R. (2018). Comparison between the NMPC and EOR control of wind turbines using LIDAR wind measurements. SCIENCE OF MAKING TORQUE FROM WIND (TORQUE 2018), 1037, (3), IOP PUBLISHING LTD. https://doi.org/10.1088/1742-6596/1037/3/032046.

Persistent Link:
http://hdl.handle.net/11343/219134

File Description:
Published version